DOI 10.4430/bgo00381

Contribution of gravity anomalies interpretation to the geology of the Jbel Saghro (eastern Anti-Atlas, Morocco): implications for the impact of structural control on sedimentation distribution

A. Idrissi[1], M. Saadi[1], Y. Astati[2], L. Harrouchi[3], J.-E. Nacer[4], A. Bouayachi[5] and K. Benyas[6]

[1] *Department of Earth Sciences, Faculty of Sciences, Mohamed V University, Rabat, Morocco*

[2] *National Office of Hydrocarbons and Mines, Rabat, Morocco*

[3] *Sahara Geology Laboratory, Kasdi Merbah University, Ouargla, Algeria*

[4] *Nuclear Research Center of Draria, Algiers, Algeria*

[5] *Department of Geology, Ben M'sik Faculty of Sciences, Hassan II University, Casablanca, Morocco*

[6] *Laboratory of Water and Natural Resources Analysis, Mohammadia School of Engineers, Mohamed V University, Rabat, Morocco*

(Received: 1 February 2021; accepted: 30 November 2021; published online: 22 March 2022)

ABSTRACT The objective of the gravity investigation in Saghro is to follow the depth of the causative sources and to examine the continuity of the geological formation boundaries. To achieve these objectives, the Bouguer anomaly data was subjected to a subtraction of the regional component and, then, interpreted in the light of three mathematical transformations. The upward-continuation enabled classifying the causative features to deep and shallow sources. Source-Parameter-Imaging allowed us to determine the depth and distribution of the basement uplifts, while the horizontal gradient was used to detect subsurface linear discontinuities, which correspond to geological lineaments. The horizontal gradient enabled revealing several faults trending mainly E-W, NE-SW, and NW-SE; these lineaments are linked to the Anti-Atlas tectonic events. The gravity analysis outcomes were validated by field investigations and interpreted in the light of the previous geological studies carried out in Saghro. The distribution of the basement uplifts is related to tectonics, which transformed the basement into high and low areas, and subsequently influenced posterior sediments distribution. The Saghro southern flank registers a thick and complete sedimentary sequence, whereas the sequence on its northern flank is thin, indicating relatively higher subsidence on the southern flank due to various faulting systems.

Key words: gravity data, Jbel Saghro, fault, anomaly, basement, eastern Anti-Atlas.

1. Introduction

The eastern Anti-Atlas is located on the northern rim of the West African Craton that exposes wide Neoproterozoic outcrops (Leblanc and Lancelot, 1980; Saquaque *et al*., 1992) surrounded by a massive Paleozoic cover. The Anti-Atlas has a complex geodynamic evolution, with numerous

tectonic events recorded during its geological history (Charrue, 2006; Baidder, 2007; Gouiza *et al*., 2017).

Several studies have provided significant information on the Anti-Atlas structural and sedimentological evolution. Despite these studies (Leblanc and Lancelot, 1980; Saquaque *et al*., 1992; Charrue, 2006; Baidder, 2007), the eastern Anti-Atlas has not been fully studied and most of its geological features remain undiscovered. In order to shed light on the geology of the eastern Anti-Atlas, a gravity data analysis was carried out in the Jbel Saghro area. The objective of this analysis is to delineate subsurface geological structures controlling the distribution of sedimentary successions and to estimate their location and depth.

To achieve this aim, the Bouguer anomaly data were processed to produce a residual anomaly map using the Oasis Montaj Software (Geosoft, 2007). The gravity lineament map, compiled from the gravity analysis, highlighted the geological structures and helped delineate the heterogeneities of the Jbel Saghro basement. The results of the gravity analysis are compatible with the field data, proving the efficacy of the current method.

2. Geological setting

The eastern Anti-Atlas is characterised by the complexity of its structural style and the diversity of its lithostratigraphy, ranging from Neoproterozoic to Cretaceous (Piqué *et al*., 2006). Due to its position on the northern rim of the West African Craton (Fig. 1), the eastern Anti-Atlas records a particular geological history and geodynamic evolution.

2.1. Neoproterozoic tectonics

The Pan-African orogeny is heterogeneous throughout the Anti-Atlas, and has been produced by several faults of various orientations (Leblanc, 1973, 1976, 1977; Leblanc and Billaud, 1978; Leblanc and Lancelot, 1980; Ennih *et al*., 2001). This orogeny has led to the assemblage of the three cratons: West African Craton, Congo Craton, and South African Craton. In the eastern Anti-Atlas, the Pan-African deformation is concentrated in E-W trending dextral shear zones (Ighid *et al*., 1989).

During the Upper Neoproterozoic, the Jbel Saghro underwent an extensive phase that probably led to an ocean basin opening (Mokhtari, 1993). Based on combinations of sedimentological analyses and synsedimentary tectonics, a NW-SE to WNW-ESE trending extension was proposed by Fekkak *et al*. (2001, 2003).

A NE-SW trending tectonic inversion occurred throughout the terminal Proterozoic, leading to the emplacement of calc-alkaline intrusions in Jbel Saghro (Mokhtari, 1993).

2.2. Paleozoic tectonics

The dislocation of the paleo-Gandowana and the opening of the paleo-Tethys ocean led to a crustal extension in the Gandowanian terrains (Stampfli and Borel, 2002). Due to this event, a Lower Cambrian rift was triggered in Moroccan lands, and structured the Anti-Atlas into horsts and grabens. In the eastern Anti-Atlas, the extension was oriented NW-SE and generated by normal NE-SW trending faults (Baidder, 2007; Hejja *et al*., 2019; Idrissi *et al*., 2021).

The Hercynian orogeny in the eastern Anti-Atlas was controlled by faults inherited from the extensive Neoproterozoic-Cambrian phase. A thick-skin tectonic inversion occurred in the

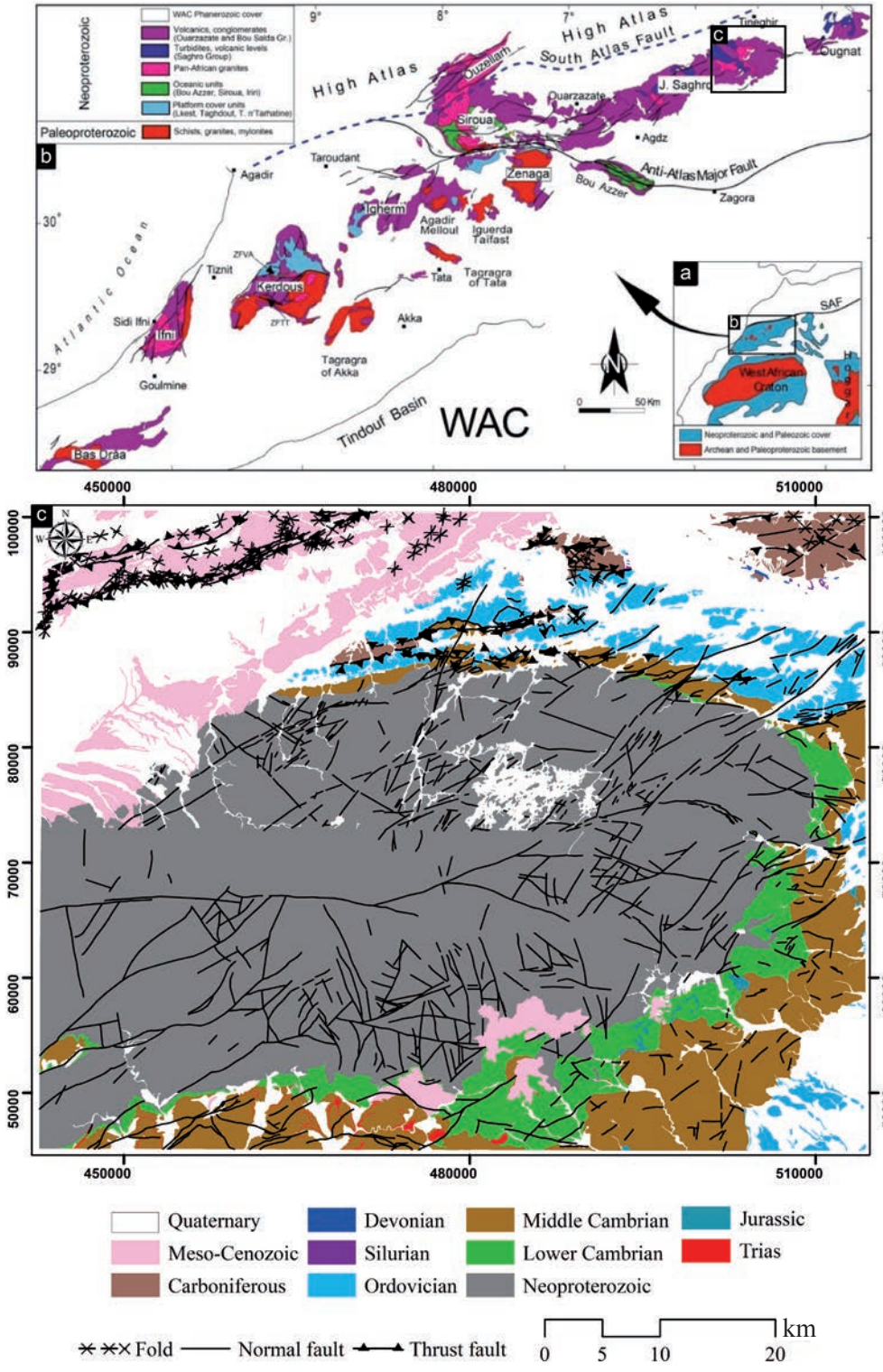

Fig. 1 - Geological map of the Anti-Atlas belt in the West African Craton (WAC) (Gasquet *et al.*, 2008): a) position of the Anti-Atlas in the WAC; b) main geological features of the Anti-Atlas belt; c) geological map (north of Morocco, Lambert projection) of the Jbel Saghro area derived from the geological maps of Imiter, Boumalne, Taghazout, Imi N'zrou, Tiwit, and Ikniwen maps of the Moroccan Geological Survey, Ministry of Energy and Mining (scale 1:50,000).

absence of major *decollement* at the basement-cover contact (Burkhard *et al*., 2006; Charrue, 2006; Baidder *et al*., 2016). The Hercynian orogeny was produced by a compressive regime of a NE-SW trending main stress (Baidder, 2007).

2.3. Meso-Cenozoic tectonics

Various studies by several authors claim that the Anti-Atlas remained stable during the post-Hercynian period (Choubert, 1952; Michard, 1976). Yet, new works have confirmed a post-Hercynian tectonic instability in the entire Anti-Atlas domain (Charrue, 2006; Baidder, 2007; Soulaimani *et al*., 2014; Gouiza *et al*., 2017).

Contemporary with the central Atlantic rifting and the Atlas rifting, and due to its position on the high edge of the rift zone during the Late Triassic to Middle Jurassic period (Soulaimani *et al*., 2014; Gouiza *et al*., 2017), the Anti-Atlas underwent an elevation of 7.5 to 10.5 km (Gouiza *et al*., 2017).

The post-rift phase from Jurassic to Lower Cretaceous corresponds to a period of the lithosphere thermal relaxation (Gouiza *et al*., 2017), which led to E-W trending tectonics (Baidder, 2007) and a subsidence rate ranging between 1 and 3 km of the Anti-Atlas basement (Gouiza *et al*., 2017).

The dislocation of the Pangea during the terminal Cretaceous to Cenozoic period by the opening of the North and South Atlantic (Stampfli and Borel, 2002), initiated the convergence and collision between Africa and Iberia/Europe. The convergence generated a compressive regime that led to the present elevation (2-3.5 km) of the Anti-Atlas via the reactivation of Precambrian and Paleozoic faults.

2.4. The Cambrian sediments record

The sedimentary formations of Lower and Middle Cambrian deposits are divided into several formations. The Lower Cambrian formations belong to the Tata group consisting of detrital and carbonate sediments, which lie unconformably on the Neoproterozoic basement. The distribution of the Lower Cambrian formations varies in the Anti-Atlas, they are complete in the western Anti-Atlas and gradually reduced towards the eastern regions.

In the eastern Anti-Atlas, the Tata group classically comprises a basal conglomerate (Landing *et al*., 2006), followed by shale and limestone intercalations referred to as the Issafene Formation, and finally the Pink Sandstone Formation (Piqué *et al*., 2006). These formations occur mainly in the SE of the Taghazout buttonhole, the south of the Imi n'Ouzrou buttonhole, the Alnif region and in the south of the Ougnat Massif. Lower Cambrian sediments are absent in the Boumalne and Imiter buttonhole, which are located in the northern flank of Jbel Saghro (Choubert, 1946; Destombes *et al*., 1985; Baidder, 2007; Hejja *et al*., 2019).

The Middle Cambrian consists of the Internal Feijas formations (Choubert, 1946). The sedimentary series begin with the discordant level of the Breccia at Micmacca, which marks the transgression of the Middle Cambrian on the Lower Cambrian deposits and on the Neoproterozoic basement. Above, the sedimentary successions continue with the Paradoxides rich Shales also called the J. Wawrmast Formation crowned by the Tabanite Sandstone Formation (Destombes *et al*., 1985).

3. Data and method

The data used in this study have been provided by the International Gravimetric Bureau (IGB) as numeric format of the complete Bouguer anomaly, published by Bosch (1972). The Bouguer

anomalies are derived from the official Earth Gravitational Model (EGM2008) released by the National Geospatial Intelligence Agency (NGA).

The Bouguer anomaly map is the result of superimposing regional and local anomalies. It is therefore necessary to separate these two components by the trend surface (Menke, 1989), a mathematical filtering procedure obtained by fitting a polynomial function using the method of least squares (in this study we used a first order equation).

Because the current study is focused on local subsurface structures, the residual anomaly map was subjected to several mathematical transformations, including the calculation of the upward continuation (UC), the application of Source Parameter Imaging (SPI), and the calculation of the horizontal gradient (HG).

3.1. Upward continuation

The UC is a mathematical technique used to attenuate short wavelengths due to surface sources or various noises. UC converts the potential field measured on one surface to the field that would be measured on another surface farther from all sources (Blakely, 1995). It is a practical operation for smoothing anomaly maps, and for assembling maps from surveys carried out at different altitudes into a single map (Blakely, 1995), in order to simplify regional interpretation (Mouge and Galdeano, 1991; Asfirane and Galdeano, 1995). The UC of the anomaly map helps highlight buried causative sources of any dimension at any depth and separate the anomalies of the deeper geology from shallower geology, by attenuating the short wavelength anomaly components and enhancing the long wavelength ones (Jacobsen, 1987; Blakely, 1995). Furthermore, the UC filter helps in sampling the gravity data according to various horizontal surfaces; in this study case, the residual gravity map was upward continued to several elevations between 1000 and 9000 m, in order to follow the vertical distribution of the anomalous features.

According to Jacobsen (1987), the UC operator is given by elementary functions in both space and wavenumber domains, is numerically stable, and can be used to build standard separation filters. Zeng *et al*. (2007) demonstrated that UC can also be used to separate a regional gravity anomaly resulting from deep sources from the observed gravity.

According to Kebede *et al*. (2020), the UC is a transformation of the gravity anomaly determined at a point, Q (x_0, y_0, $z_0 = 0$); on the mean sea level to a point p (x_0, y_0, $z_0 = -h$), on some higher flat surface upward continued to $z = -h < 0$ (Fig. 2).

The gravitational attraction per unit mass of a causative source, *dm*, at mean see level, Q (x_0, y_0, $z_0 = 0$), at distance *R* from the source location point Q (x, y, z), is given by:

$$dg = \frac{Gdm}{R^2} = \frac{Gdm}{(x-x_0)^2+(y-y_0)^2+(z-z_0)^2} \quad (1)$$

In terms of practical manipulation, the residual anomaly map was used as an input in the MAGMAP Tool of Oasis Montaj Software (version 8.4). Since the residual map was upward continued following various elevations, the UC operation was repeated several times. Accordingly, nine upward continuation residual anomaly maps have been generated in this section, each representing the variation of the anomalous features at the corresponding UC height.

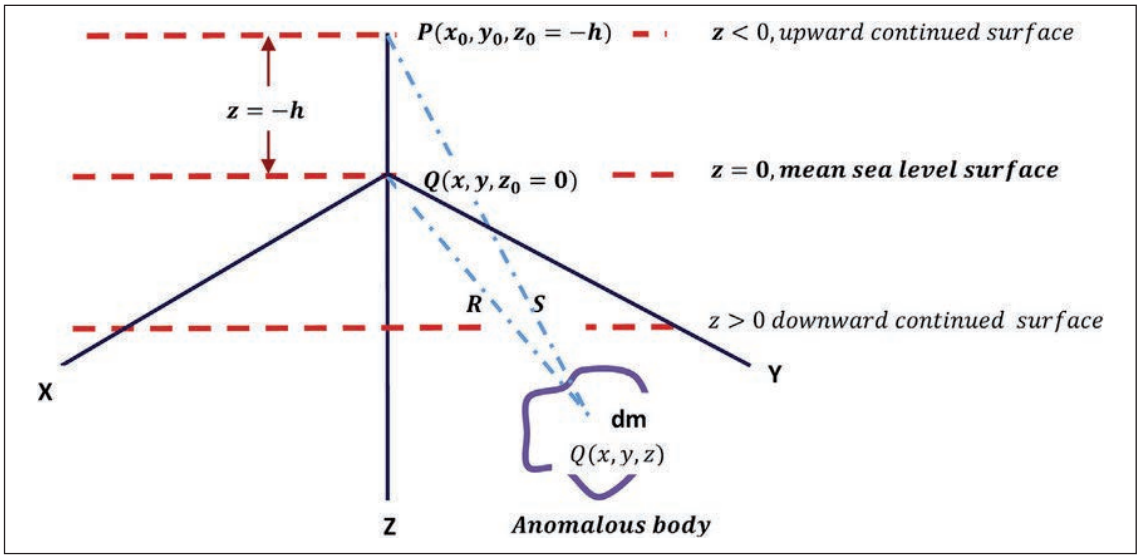

Fig. 2 - Pictorial representation of UC technique in Cartesian coordinate system (Kebede *et al*., 2020).

3.2. Source Parameter Imaging

SPI is a fast and efficient function to determine the depth of gravity and magnetic sources (Nabighan, 1972) using an extension of the complex analytical signal. The SPI was developed by Thurston and Smith *et al*. (1997), and has been used extensively by Thurston and Smith (1997) and Salako (2014). The method uses the relationship between the observed field local wavenumber (*k*) defined as the rate of change of the phase of the analytic signal (Bracewell, 1965) and the source depth, which can be calculated for any point within a grid of data via horizontal and vertical gradients. At peaks in the local wavenumber grid, the source depth is equal to (*n*+1)/*k*, where *n* depends on the assumed source geometry. Peaks in the wavenumber grid are identified using a peak tracking algorithm and valid depth estimates are isolated (Blakely and Simpson, 1986). The advantages of the SPI method are that no moving data window is involved and the computation time is relatively short. Also for magnetic data treatment, the SPI method is independent of remanent magnetisation or other magnetic parameters like inclination, declination, dip, and strike. However, the SPI method requires the first- and second-order derivatives of the anomaly field (to obtain the first- and second-order wave numbers), which can amplify noise in the data and be affected by interference (Phillips, 2000). On the other hand, errors due to this noise can be reduced by careful filtering of the data before depths are calculated. The outcome of the SPI is an image (Smith *et al*., 1998) that indicates the estimated depth and shape of anomalous features using an automatic application on SPI software included in the Oasis Montaj Package (version 8.4).

The SPI has the advantage of providing a more complete set of coherent solution points and is easier to use. The SPI resulting image can be easily interpreted according to Thurston and Smith (1997).

The SPI transformation is carried out through several automatic mathematical processes from several grids. The application of SPI method needs the following:

- GRD1: grid of the horizontal derivative in the X-direction;
- GRD2: grid of the horizontal derivative in the Y-direction;

- GRD3: grid of the first vertical derivative;
- GRD4: grid of tilt derivative;
- GRD5: grid of local wavenumber *k* grid (horizontal gradient of tilt derivative).

The SPI technique assumes a step-type source model. The following formula holds:

$$\text{Depth} = 1/k_{max} \tag{2}$$

where k_{max} represents the peak value of *k,* which located over the step source (Smith *et al*., 1998):

$$K = \sqrt{(\frac{dA}{dx})^2 + (\frac{dA}{dy})^2} \tag{3}$$

where *A* is tilt derivative given as (Fairhead, 2011):

$$A = atan \frac{(\frac{dg}{dz})}{\sqrt{(\frac{dg}{dx})^2 + (\frac{dg}{dy})^2}} \tag{4}$$

g is the total magnetic field anomaly grid.

3.3. Horizontal gradient

Horizontal gradient is a powerful technique that helps to detect lateral density variation, which may be related to structural accidents and abnormal contacts of any orientation (Cordell, 1979; Blakely and Simpson, 1986; Amiri, 2011; Azaiez *et al*., 2011; Dufréchou *et al*., 2013; Gabtni *et al*., 2013; Nait Bba *et al*., 2019). The horizontal gradient amplitude was developed by Cordell and Grauch (1985), and is defined by the following equation:

$$GH(x,y) = \sqrt{(\frac{dG}{dx})^2 + (\frac{dG}{dy})^2} \tag{5}$$

where *G* is the field strength measured at (*x*, *y*), and *dx* and *dy* are the first horizontal derivative following respectively *x* and *y*.

The horizontal gradient operator is widely used in mapping major structural boundaries, which are poorly exposed or completely buried. This technique highlights poorly known structures, which may have major tectonic significance (Sharpton *et al*., 1987).

The resulting map was used in the structural analysis of the site, which is discussed later in the text.

3.4. Geological field surveys

The lack of previous geophysical surveys and deep wells in the study area made it difficult to interpret and validate the results obtained from the gravity data analysis. Therefore, the verification of the thicknesses of the sedimentary succession in the field was necessary. We carried out several field missions to establish nine cross-sections separated by a few kilometres within Jbel Saghro, and analysed the repartition of the basement uplifts (Table 1).

Table 1 - Details of the gravimetric survey.

Survey details	**Characteristics**
Reference station	Elevation 455.6 m Latitude 31° 38.0’ N Longitude 08° 01.0’W
Density used for data raw data reduction (g/cm3)	2.67
Survey accuracy	+ - 0.3 mGal
Date of the survey	1965

4. Results and interpretation

4.1. Gravity data analysis

The first phase in quantitative analysis of a gravity data is the separation of the Bouguer anomaly into its regional and residual.

4.1.1. Bouguer anomaly map

Based on gravity data, the Bouguer anomaly map of the Jbel Saghro eastern Anti-Atlas was generated. The map has been plotted using the minimum curvature interpolation method (Fig. 3).

This map shows anomalies of various forms, organisations, orientations, and intensities. The gravity field values range from -166 and -58 mGal, the anomalies are elongated in predominantly E-W to ESE-WNW directions. The intensity of the Bouguer anomalies decreases from south to north, showing minimal values to the NE of the map.

4.1.2. Residual anomaly map

The residual anomaly map (Fig. 4), obtained by subtracting the regional component from the Bouguer anomaly using the trend surface (previously mentioned), shows values ranging between -20.1 and 23 mGal. Based on the geological knowledge of the region, a qualitative interpretation of the anomalies can be made. The origin of the positive and negative anomalies is associated respectively with the heterogeneity (metamorphic rocks, granitoides, and granite) of the outcropping basement and the location of the sedimentary basins (Fig. 5). This mainly means that more the basement rocks are exposed, the more the density contrast is evident, but when the basement is hidden by sedimentation, the contrast is unnoticeable.

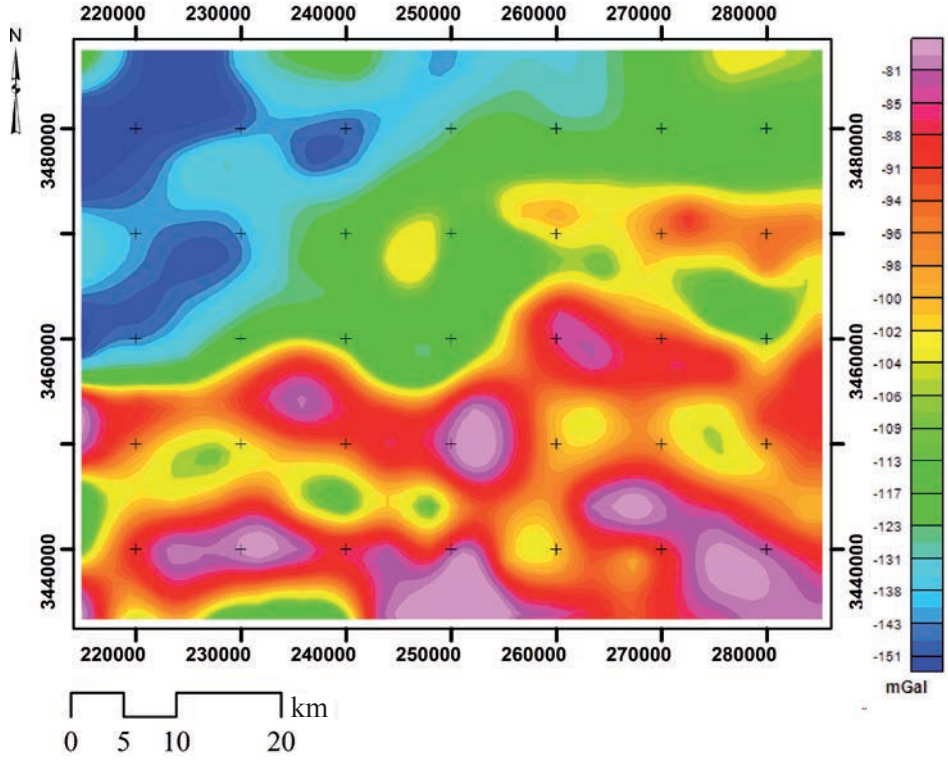

Fig. 3 - The Bouguer anomaly map of Jbel Saghro (UTM projection).

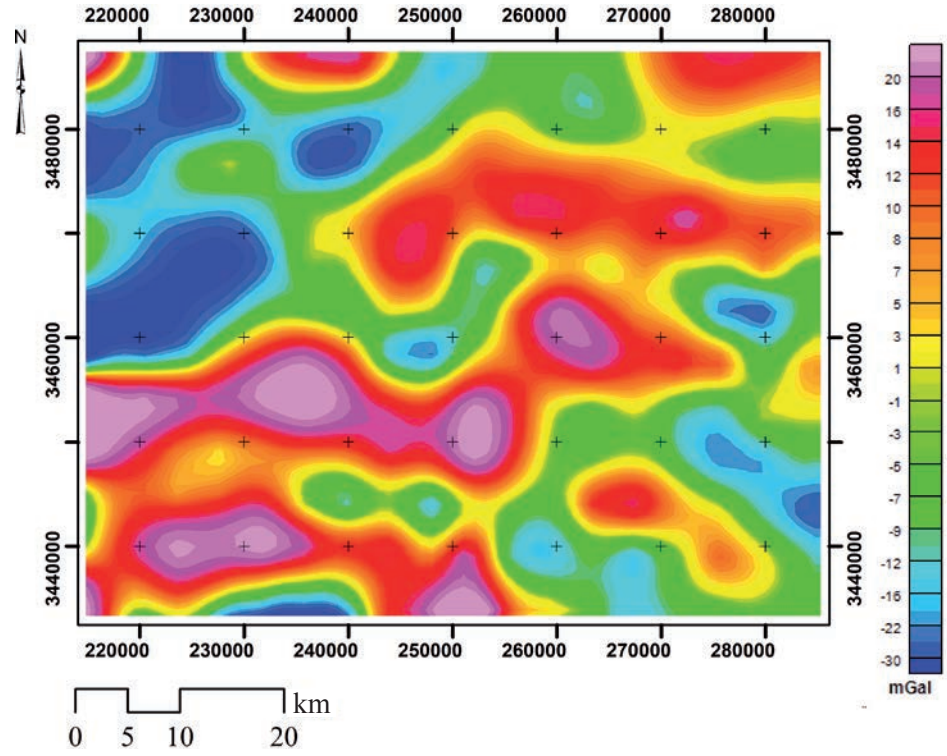

Fig. 4 - The residual anomaly map of Jbel Saghro.

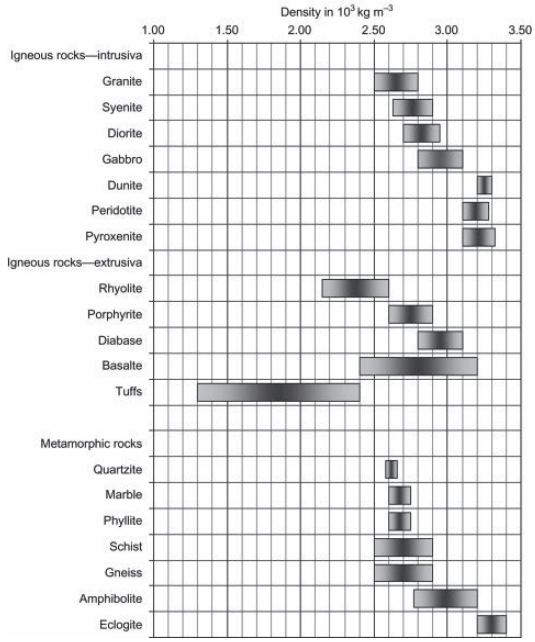

Fig. 5 - Density values of some igneous and metamorphic rocks (after Schön, 2015).

The residual map shows the distribution of positive anomalies (red colour) in the north-eastern and south-western regions of the Jbel Saghro trending generally E-W to ESE-WNW. The location of the anomalies coincides with the location of crystalline Neoproterozoic basement rocks.

While the negative anomalies (blue colour) are located in the north-western and south-eastern parts of Jbel Saghro, oriented NE-SW and NW-SE respectively. The negative anomalies are located underneath the low-density rocks of the Meso-Cenozoic cover.

4.1.3. Upward continuation

In this work, the UC was used to highlight the depth of the anomalous sources, and the residual gravity map was upward continued to a height of 1000, 3000, 5000, 7000, and 9000 m (Fig. 6).

The UC maps highlight long wavelength anomalies. The shape and extension of the anomalies are presented in function of the UC altitude. The analysis of the UC maps reveals that the amplitude of the anomalies decreases or disappears as the height of the UC increases. By increasing the altitude from 1000 to 9000 m, the behaviour of the anomalous features varies in three different ways. Some positive anomalies interfere with each other and merge under one single anomaly, as in the case of (A6, A5, and A4); other intensities decreased (A3 and A1), while some anomalies gradually decrease until disappearing (A7 and A2). The UC of the residual anomaly map allowed distinguishing the anomalies attributed to surface sources (depth between 1000 and 3000 m) from those of deeper origin (depth > 9000 m), and designated the anomalies that have the same origin (depth between 5000 and 7000 m).

The origin of the causative sources is the basement rocks. The differential distribution of the basement uplifts generated a modification of the sources depth - low areas of the basement are deep, while the high areas are exposed, which explains the depth variation of the anomalous sources.

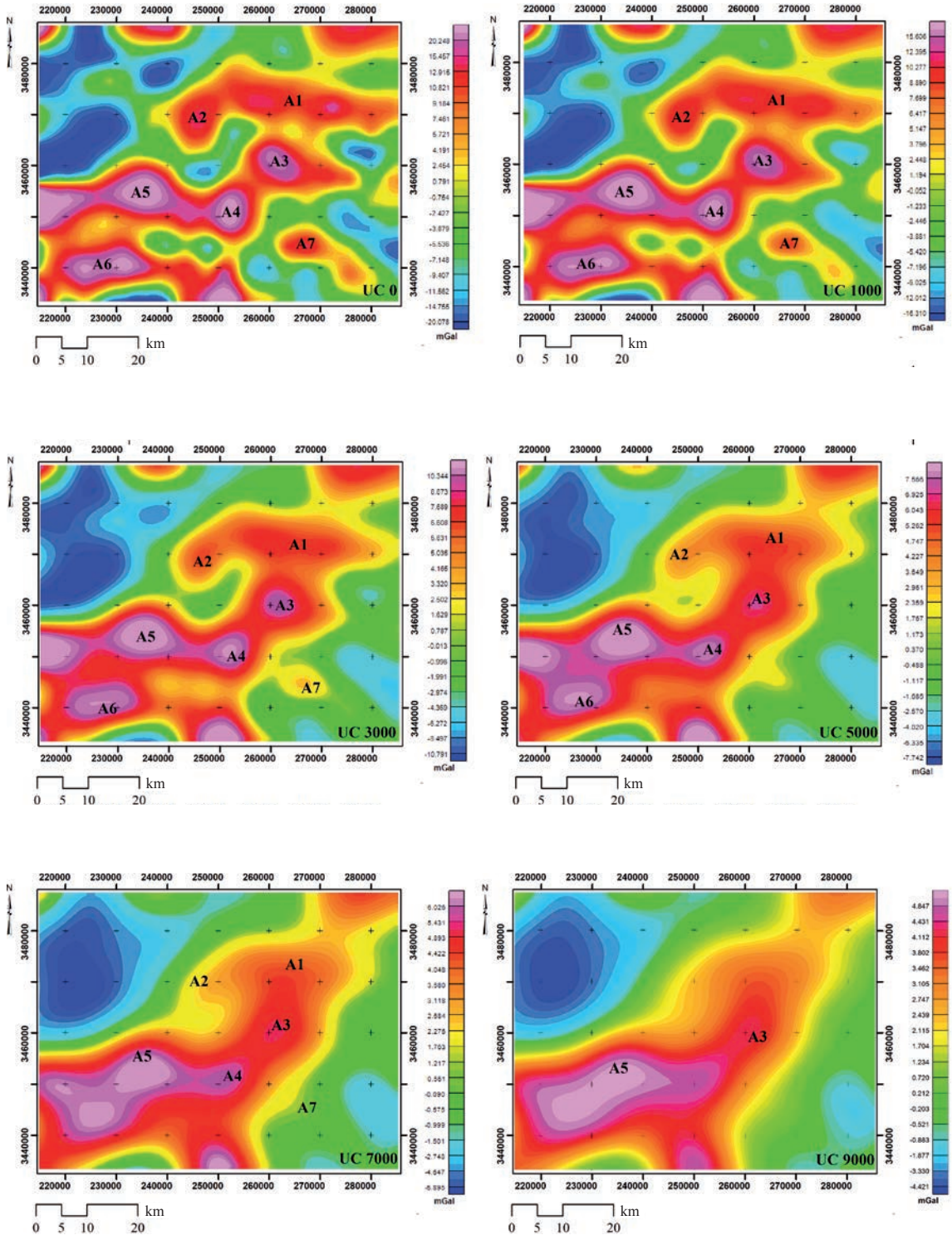

Fig. 6 - The residual anomaly map of the Jbel Saghro upward continued to different altitudes (UC is the value of UC altitude in metres).

4.1.4. Source Parameter Imaging

The map produced by SPI transformation (Fig. 7) reveals variable depths ranging between 637 and 3495 m. In comparison with the geological map and the field studies, the shallower depths coincide with the basement outcrops (blue colour), and the deeper depths coincide with the profounder sources hidden by the Paleozoic and Meso-Cenozoic sedimentation sites (red colour).

The Jbel Saghro basement is characterised by the heterogeneity of its rocks, including Middle Neoproterozoic granitoids and dense metamorphic rocks, overlaid by Upper Neoproterozoic andesites and conglomerate deposits (Leblanc, 1976; Aït Malek *et al*., 1998; Piqué, 2003). The distribution of Upper Neoproterozoic deposits locally conceals earlier terrains, which explains the increase in depth of anomalous sources even at the basement level. Field verification reveals the existence of enormous Upper Neoproterozoic conglomerate benches (Fig. 7), which cover the high density rocks deposited earlier. This would explain the great depth of the causative sources in the basement areas.

The SPI map delineates sedimentary depressions as well, such as the Tisdafine basin (composed of calcareous rocks) located in the extreme NE, the Cambrian basin situated in the SE, and Meso-Cenozoic deposits in the north and NE (Fig. 7).

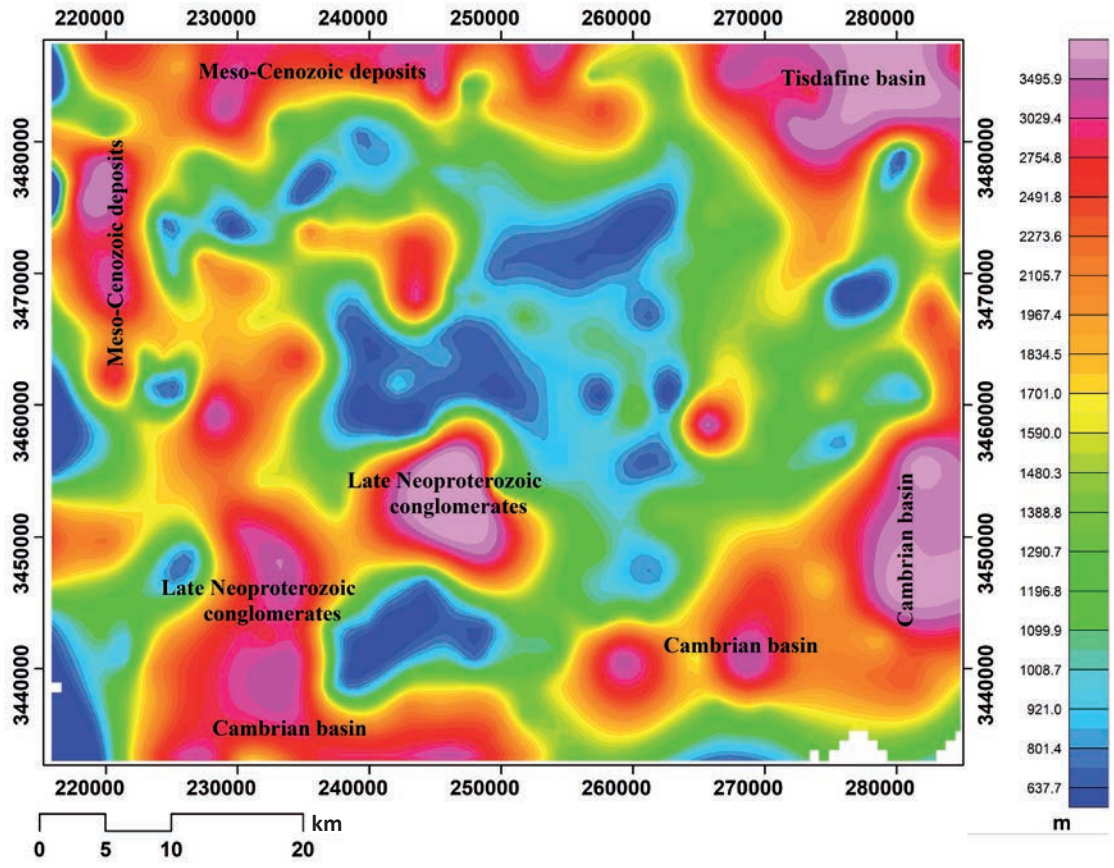

Fig. 7 - The SPI map showing the depths distribution of causative sources.

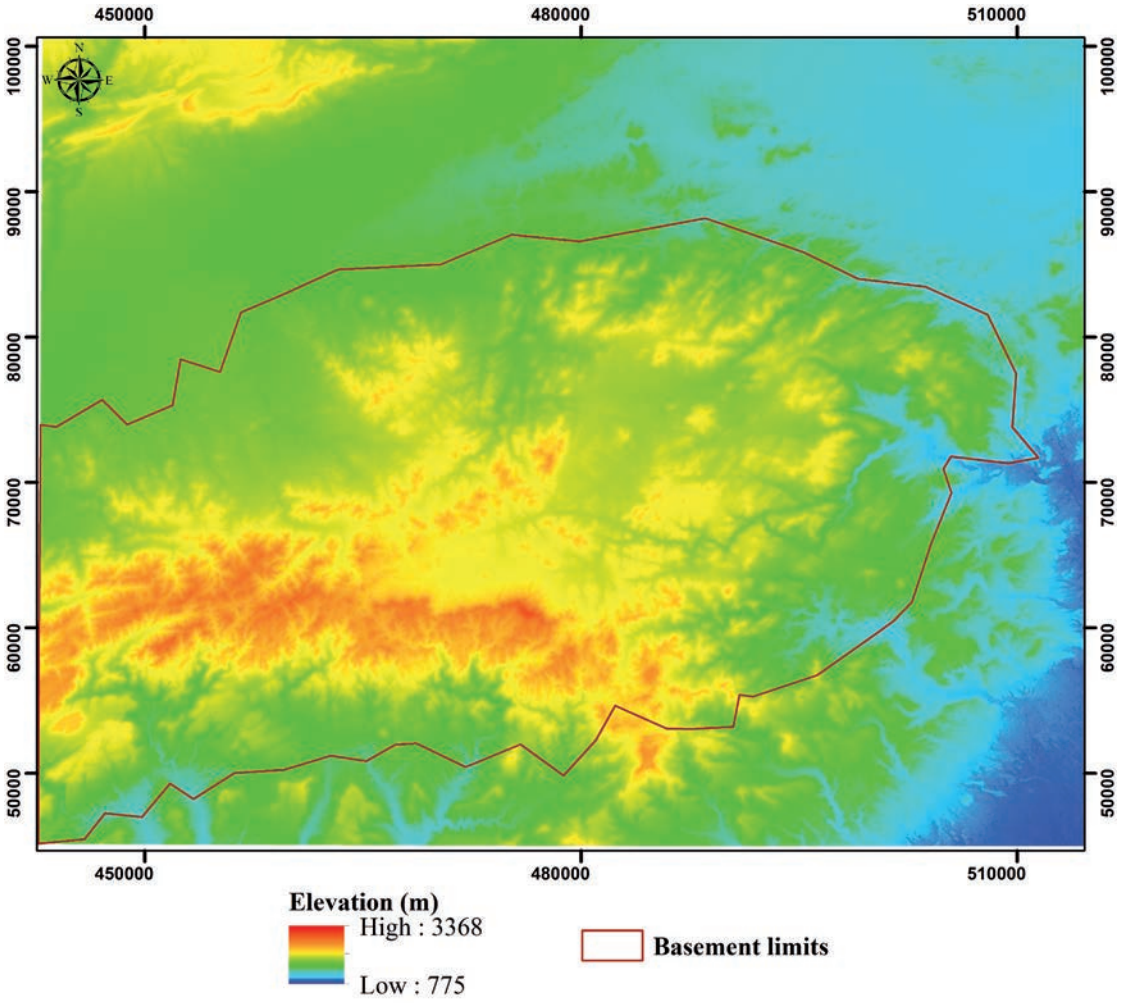

Fig. 8 - DEM of the Saghro area.

The distribution of Precambrian basement uplifted blocks influences the repartition of post-Neoproterozoic sedimentation along the Jbel Saghro. A verification of the thickness of the sedimentary series in the field was necessary to validate the outcomes of the gravity data analysis.

The Digital Elevation Model (DEM) of the study area (Fig. 8) represents the elevation data of the Jbel Saghro terrains. The DEM presents the reliefs of the study area and designates their altitude.

According to Fig. 8, the topography is high where the basement is located and low where the sedimentary basins are situated. This indicates the differential distribution of the basement uplifts, which has been confirmed using the geophysical methods of this study.

4.2. Detection of subsurface discontinuities: horizontal gradient

The horizontal gradient is used to locate approximate boundaries corresponding to geological contacts or faults from gravity data. Linear contacts correspond to faults, while circular contacts are the boundaries of intrusive bodies (Vanié *et al.*, 2005). The statistical analysis of the horizontal

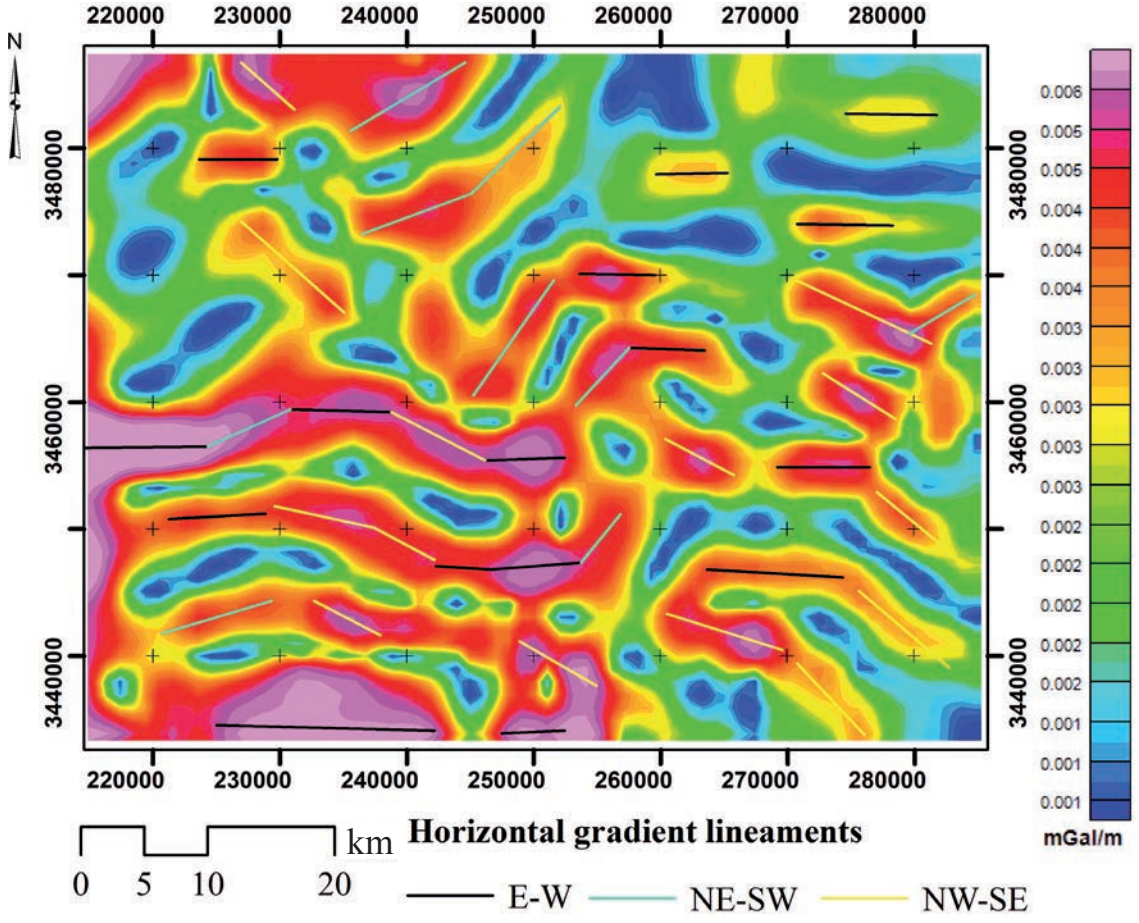

Fig. 9 - Horizontal gradient map of the Jbel Saghro.

gradient map shows three major faulting trends, listed in order of dominance: E-W, NE-SW, and NW-SE.

The E-W family is frequently located in the SW and central part of the map, it is characterised by extended lineaments, which limit the high-density bodies in the region. The E-W family crosses most of the Jbel Saghro terrains, and corresponds to east-trending faults of the post-Hercynian phase (Baidder, 2007) resulting from the post-rift phase of the central Atlantic (Gouiza *et al*., 2017).

The NE-SW lineaments are located in the NW, the middle and in the SE of the map. The lineaments are less extensive and delineate the anomalous sources as well. These lineaments are located at the basement-cover contact, and can be interpreted based on previous work, as inherited faults from the extensive Cambrian phase (Baidder, 2007; Hejja *et al*., 2019; Idrissi *et al*., 2021).

The NW-SE faults are dispersed throughout the study area. According to several authors (Mokhtari, 1993; Soulaimani *et al*., 2014; Hejja *et al*., 2019; Idrissi *et al*., 2021), this family corresponds to normal faults responsible for the extension of the Upper Neoproterozoic in the Saghro Massif, based on combinations of sedimentological analyses and synsedimentary tectonics (Mokhtari, 1993; Fekkak *et al*., 2001; Fekkak *et al*., 2003).

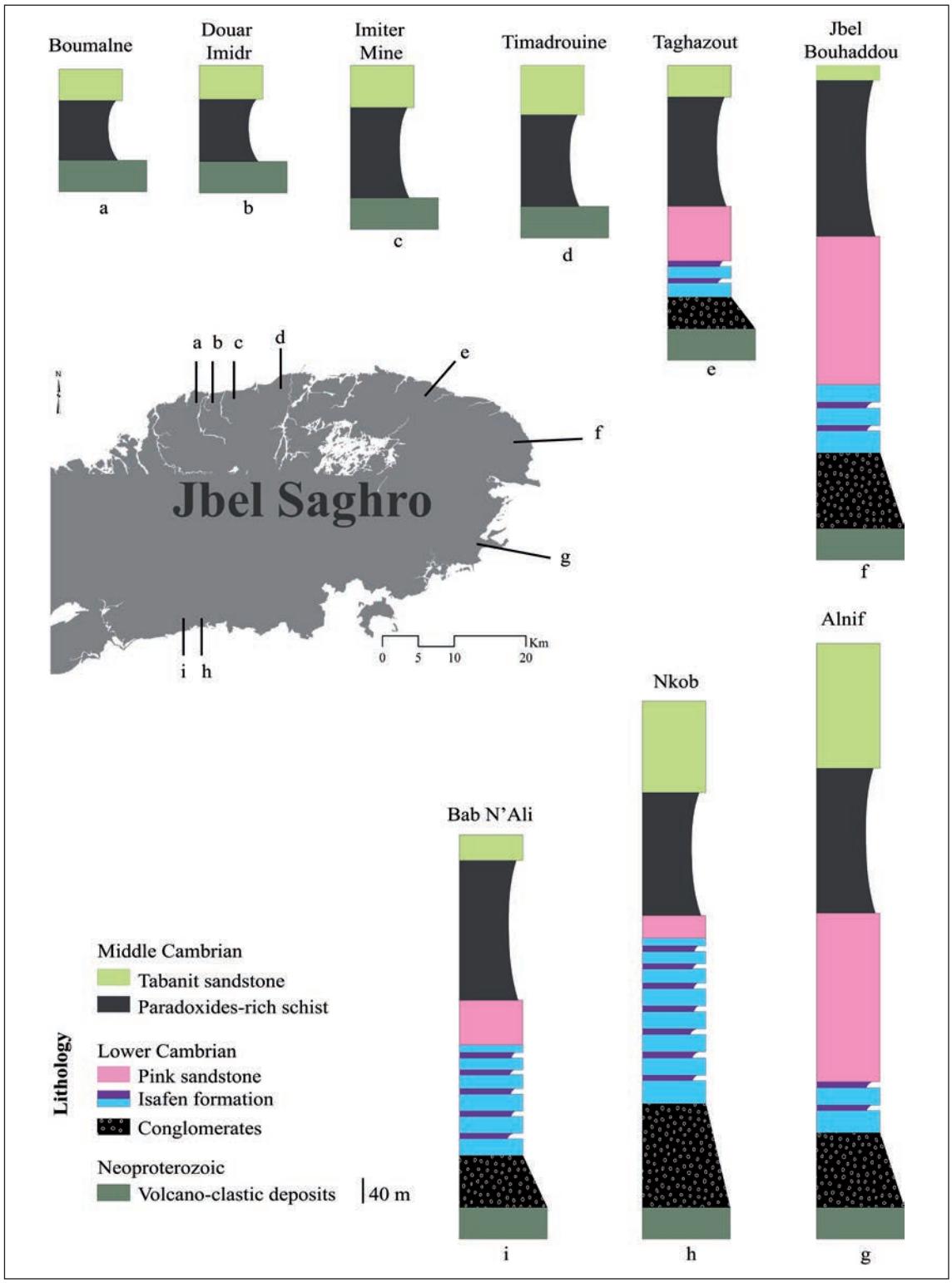

Fig. 10 - Lithostratigraphic sections showing the variation in thickness of Cambrian sediments around Jbel Saghro (the elevations of the sections according to the geological map of Jbel Saghro are: a) 1500 m; b) 1500 m; c) 1500 m; d) 1500 m; e) 1493 m; f) 1480 m; g) 1490 m; h) 1700 m; i) 1700 m).

4.3. Field validation

In order to verify the results of the gravity data analysis, we carried out several field missions. The study area displays hiatus, dissimilar sedimentation thickness, and outcropping basement uplifts. To highlight these variations, we logged 9 distanced lithostratigraphic sections around the Jbel Saghro basement. The sedimentary survey helped identify the basement topography variation in the field and showed the dominance of tectonic control on the sedimentation rate.

The sections logged show thickness dissimilarities along the Jbel Saghro (Fig. 10): the northern flank deposits are thinner than those of the southern flank, indicating a differential distribution of basement uplifts, and thus the influence of tectonics on the basement and its posterior sedimentary cover.

Based on our structural mapping and the existing geological maps of Jbel Saghro (scale 1:50,000), the fractures are mainly oriented: NE-SW, E-W, and NW-SE (Fig. 11). The comparison between the rose diagram of structural fractures and the horizontal gradient lineaments trending shows a significant orientation similarity.

5. Discussion

Gravity data analysis is an efficient method to highlight deep faults, their limits and ramifications (Everaerts and Mansy, 2001), as well as the topography of the basement below the sedimentary cover. The analysis of gravity data of the study area allowed us to highlight various geological structures of Jbel Saghro, which are partially or totally hidden by the sedimentary cover.

The application of the horizontal gradient method, enabled detecting several lineaments corresponding to known faults identified by the previous structural field studies, consisting of three main families of regional gravity lineaments trending E-W, NW-SE, and NE-SW. These faulting systems are in good agreement with the results of classical structural studies (Mokhtari, 1993; Charrue, 2006; Baidder, 2007; Soulaimani *et al*., 2014).

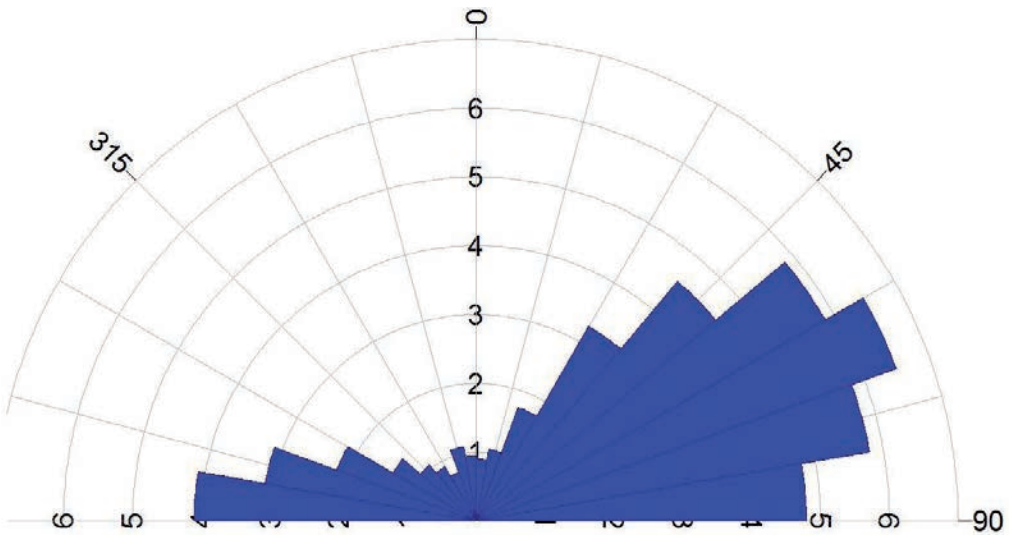

Fig. 11 - Rose diagram of structural data of Jbel Saghro.

According to the gravity anomaly combinations, their reflecting structural properties, and field investigations, we identified the trend, the type, and the length of the mapped faults. These faults correspond to an extensive structural style, which is the most common in the study area, represented mainly by normal faults caused by the extensional tectonic stress field.

The NW-SE trend corresponds to inherited faults, mainly affecting the Neoproterozoic basement and causing its topography variation. The geodynamic evolution during the late Neoproterozoic era was controlled by an extensive main stress that led to the formation of graben and horst structures throughout the entire Anti-Atlas.

NE-SW trending lineaments are dominant in the Jbel Saghro area and are well documented and interpreted as related to the Cambrian rifting. These structures are synsedimentary faults and caused the sedimentary sequence thickness variation. In the field, the faults cause the displacement and dislocation of strata, which also cause density differences and thus gravity anomalies. Field measurement reveals a NE dip direction, which is conformable with the sedimentological record. The sequences in the NE of the NE-SW trending faults are thicker than those to the NW, and the basement also outcrops in the NW and is buried under the sedimentary cover towards the NE of these faults.

E-W trending faults are interpreted as the consequences of post Hercynian orogeny extension, and they crosscut the Neoproterozoic and the Paleozoic terrains. Their effect is low to moderate in the study area compared to the NE-SW and the NW-SE trending faults, and they are rarely associated with hydrothermal quartz.

The superposition of gravity derived lineaments with fault-systems, mapped by previous geological studies (Fig. 12), allowed us to confirm the existence of some faults that were already mapped by surface structural studies, as well as mapping and specifying new major blind faults that have not been recognised before. However, in many parts of the Jbel Saghro area, some geological fault-systems do not appear in our geophysical filtering due to the low density contrast between the adjacent blocks.

The identification of the anomaly depths, caused by the basement uplifts, allowed us to identify the Precambrian basement topography, and to explain the variation in thickness of the sedimentary cover. This is validated by field investigations, which have surveyed the thickness of the sedimentary series around the basement. These thicknesses are highly reduced and even absent and less significant in the north compared to the south of Saghro, where Cambrian series are complete and well developed. This indicates a differential distribution of Precambrian basement uplifts, and thus the influence of tectonics on the structuring of the basement and on the subsequent sedimentation.

Therefore, we can deduce that the subsurface geometry of the study area is configured by many faults that organised the basement into low and high areas. The mapped gravity structures correspond to the main tectonic trends that controlled the study area evolution during the Neoproterozoic-early Paleozoic period.

The Anti-Atlas domain underwent several geological events throughout the early and middle Neoproterozoic, where the terrains were deformed by the Pan-African orogeny. The late Neoproterozoic instead corresponds to the destruction and erosion of the Pan-African belt, and the deposition of the synrift sediments derived from the eroded Pan-African reliefs (Piqué *et al*., 1999; Piqué, 2003; Soulaimani *et al*., 2003). From the latest Neoproterozoic to the beginning of the Paleozoic, a structural extension occurred and developed fault-limited basins, as a result of the stretching of the continental crust (Piqué, 2003). The crustal extension was shown by the development of grabens where the Cambrian marine transgression progressed, while horsts remained emerged.

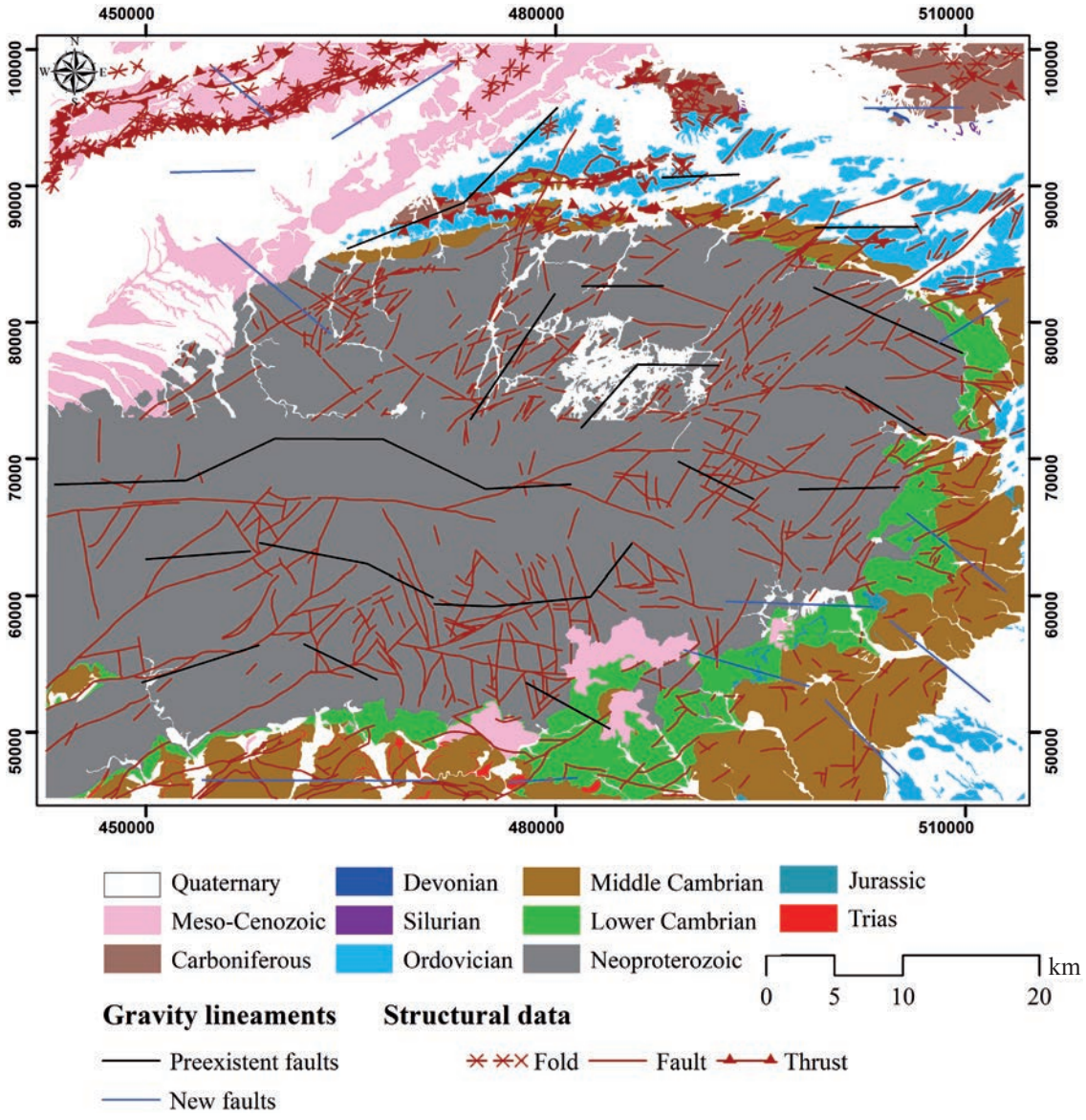

Fig. 12 - Geological map of Jbel Saghro (scale 1:50,000) showing the main structural features of the study area and the projection of the gravity lineaments.

6. Conclusions

This work presents the analysis of gravity data of the Jbel Saghro area. The map of the Bouguer anomaly includes regional and residual anomalies, hence the importance of the separation by the polynomial method. The residual anomaly map was used as a base map for the geophysical treatments.

The results of the horizontal gradient treatment indicate the presence of three faulting systems: the E-W trend, which corresponds to the E-W striking faults of the extensive post-Hercynian phase; the NE-SW trend from the Cambrian extension, and the NW-SE trend inherited from the extensive Upper Neoproterozoic events. These latter two trending faults are responsible

for the structuration of the Precambrian basement into high and low areas, which controlled the sedimentation rate of the Paleozoic cover.

The application of the UC on the residual Bouguer anomaly map allowed identifying the depth of the anomalous sources and following their vertical distribution in order to separate the shallow anomalies from the deeper ones. The results of the SPI transformation highlighted the spatial distribution of the anomalies, thus indicating the spatial organisation of the basement uplifts that, consequently, influenced the posterior sedimentation. The results of the gravity data interpretation are compatible with the field investigations, whereby the lateral and spatial distribution of the anomalies corresponds to the basement rocks location identified in the field. The sections logged and the observations noted made it possible to interpret and validate the outcomes of the geophysical treatment, hence demonstrating the effectiveness of this method.

REFERENCES

Aït Malek H., Gasquet D., Bertrand J.M. and Leterrier J.; 1998: *Géchronologie U-Pb sur zircon de granitoïdes éburnéens et panafricains dans les boutonniers protérozoïque d'Igherm, du Kerdous et du Bas Drâa (Anti-Atlas occidental, Maroc)*. C. R. Acad. Sci., 327, 819-826.

Amiri A., Chaqui A., Hamdi I., Inoubli M.H., Ben Ayed N. and Tlig S.; 2011: *Role of preexisting faults in the geodynamic evolution of northern Tunisia, insights from gravity data from the Medjerda Valley*. Tectonophys., 506, 1-10.

Asfirane F. and Galdeano A.; 1995: *The aeromagnetic map of northern Algeria: processing and interpretation*. Earth Planet. Sci. Lett., 136, 61-78, doi: 10.1016/0012-821X(95)00043-4.

Azaiez H., Gabtni H., Bouyahya I., Tanfous D., Haji S. and Bedir M.; 2011: *Lineaments extraction from gravity data by automatic lineament tracing method in Sidi Bouzid basin (central Tunisia): structural framework inference and hydrogeological implicatio*n. Int. J. Geosci*.,* 2, 373-383.

Baidder L.; 2007: *Structuration de la bordure septentrionale du Craton Ouest Africain du Cambrien à l'actuel: cas de l'Anti-Atlas oriental du Maroc*. PH.D. Thesis in Sciences, Université Hassan II Aïn Chock, Casablanca, Morocco, 210 pp.

Baidder L., Michard A., Soulaimani A., Fekkak A., Eddebbi A., Rjimati E.-C. and Raddi Y.; 2016: *Fold interference pattern in thick-skinned tectonics; a case study from the external Variscan belt of eastern Anti-Atlas, Morocco*. J. Afr. Earth Sci., 119, 204-225, doi: 10.1016/j.jafrearsci.2016.04.003.

Blakely R.J.; 1995: *Potential theory in gravity and magnetic applications*. Cambridge University Press, Cambridge, UK, 461 pp., doi: 10.1017/CBO9780511549816.

Blakely R.J. and Simpson R.W.; 1986: *Approximating edges of source bodies from magnetic or gravity anomalies*. Geophys., 51, 1494-1498, doi: 10.1190/1.1442197.

Bracewell R.N.; 1965: *The Fourier transform and its applications*. McGraw Hill Inc., New York, NY, USA, 624 pp.

Burkhard M., Caritg S., Helg U., Robert-Charrue C. and Soulaimani A.; 2006: *Tectonics of the Anti-Atlas of Morocco*. C. R. Geosci., 338, 11-24, doi: 10.1016/j.crte.2005.11.012.

Charrue C.R.; 2006: *Géologie structurale de l'Anti-Atlas oriental, Maroc*. PH.D. Thesis in Geological Sciences, Institut de Géologie et d'Hydrogéologie, Université de Neuchâtel, Switzerland, 180 pp.

Choubert G.; 1946: *Aperçue de la géologie marocaine.* Rev. Géogr. Marocaine, 2-3, 59-77.

Choubert G.; 1952: *Histoire géologique du domaine de l'Anti-Atlas*. In: Proc. 19e Congrès Géologique International, Algiers, Algeria, Vol. 6, pp. 77-194.

Cordell L.; 1979: *Gravimetric expression of graben faulting in Santa Fe country and the Espanola basin, New Mexico*. In: Guidebook to Santa Fe Country, Ingersoll R.V. (ed), 30th Field Conference, Geological Society, Socorro, NM, USA, pp. 59-64.

Cordell L. and Grauch V.J.S.; 1985: *Mapping basement magnetization zones from aeromagnetic data in the san Juan basin, New Mexico*. In: The utility of regional gravity and magnetic anomaly maps, Hinze W.J. (ed), Society of Exploration Geophysicists, Tulsa, OK, USA, pp. 181-197, doi: 10.1190/1.0931830346.ch16.

Destombes J., Hollard D. and Willefert S.; 1985: *Lower Palaeozoic rocks of Morocco*. In: Lower Palaeozoic rocks

of north-western and west-central Africa, Holland C.H. (ed), John Wiley and Sons Ltd., Chichester, UK, pp. 91-336.

Dufréchou G., Harris L.B. and Corriveau L.; 2013: *Tectonic reactivation of transverse basement structures in the Grenville orogeny of SW Quebec, Canada: insights from gravity and aeromagnetic data*. Precambrian Res., 241, 61-84.

Ennih N., Laduron D., Greiling R.O., Errami E., de Wall H. and Boutaleb M.; 2001: *Superposition de la tectonique éburnéenne et panafricaine dans les granitoïdes de la bordure nord du craton ouest africain, boutonniére de Zenaga, Anti-Atlas central, Maroc*. J. Afr. Earth Sci., 32, 677-693, doi: 10.1016/S0899-5362(02)00048-9.

Everaerts M. and Mansy J.L.; 2001: *Le filtrage des anomalies gravimetriques; une cle pour la comprehension des structures tectoniques du Boulonnais et de l'Artois (France)*. Bull. Soc. Geol. Fr., 172, 267-274, doi: 10.2113/172.3.267.

Fairhead J.D.; 2011: *Gravity and magnetics in today's oil and minerals industry.* Getech Group, Univ. of Leeds, Leeds, UK, Course notes, 321 pp.

Fekkak A., Pouclet A., Ouguir H., Ouazzani H., Badra L. and Gasquet D.; 2001: *Géochimie et signification géotectonique des volcanites du Cryogénien inférieur du Saghro (Anti-Atlas oriental, Maroc) / Geochemistry and geotectonic significance of Early Cryogenian volcanics of Saghro (eastern Anti-Atlas, Morocco).* Geodin. Acta, 14, 373-385, doi: 10.1080/09853111.2001.10510730.

Fekkak A., Pouclet A. and Benharref M.; 2003: *The middle Neoproterozoic Sidi Flah Group (Anti-Atlas, Morocco): synrift deposition in a Pan-African continent/ocean transition zone.* J. Afr. Earth Sci., 37, 73-87, doi: 10.1016/S0899-5362(03)00049-6.

Gabtni H., Jallouli C., Mickus K.L. and Turki M.M.; 2013: *Geodynamics of the southern Tethyan margin in Tunisia and Maghrebian domain: new constraints from integrated geophysical study*. Arabian J. Geosci., 6, 271-286.

Gasquet D., Ennih N., Liegeois J.P., Soulaimani A. and Michard A.; 2008: *The Pan-African belt*. In: Continental evolution: the geology of Morocco, Michard A., Saddiqi O., Chalouan A. and Frizon Lamotte D. (eds), Lecture notes in Earth sciences, Springer, Berlin, Heidelberg, Germany, vol. 116, pp. 33-64, doi: 10.1007/978-3-540-77076-3_2.

Geosoft Inc.; 2007: Oasis Montaj, Toronto, ON, Canada, <www.geosoft.com/media/uploads/resources/brochures/OM_b_2008_10_web.pdf>.

Gouiza M., Charton R., Bertotti G., Andriessen P. and Storms J.E.A.; 2017: *Post-Variscan evolution of the Anti-Atlas belt of Morocco constrained from low-temperature geochronology*. Int. J. Earth Sci., 106, 593-616, doi: 10.1007/s00531-016-1325-0.

Hejja Y., Baidder L., Ibouh H., Bba A.N., Soulaimani A., Gaouzi A. and Maacha L.; 2019: *Fractures distribution and basement-cover interaction in a polytectonic domain: a case study from the Saghro Massif (eastern Anti-Atlas, Morocco).* J. Afr. Earth Sci., 162, 103694, doi: 10.1016/j.jafrearsci.2019.103694.

Idrissi A., Saadi M., Manar A., Astati Y., Harrouchi L. and Nacer J.E.; 2021: *Contribution of aeromagnetic cartography and lithostratigraphic studies to the identification of blind faults and the Cambrian deposits geometry in Jbel Saghro (eastern Anti-Atlas, Morocco)*. Boll. Geof. Teor. Appl., 62, 101-118, doi: 10.4430/bgta0335.

Ighid L., Saquaque A. and Reuber I.; 1989: *Plutons syn-cinématiques et la déformation panafricaine majeure dans le Saghro occidental (boutonnière d'Imiter, Anti-Atlas, Maroc)*. C. R. Acad. Sci., 309, 615-620.

Jacobsen B.H.; 1987: *Case for upward continuation as a standard separation filter for potential-field maps*. Geophys., 52, 1138-1148.

Kebede H., Alemu A. and Fisseha S.; 2020: *Upward continuation and polynomial trend analysis as a gravity data decomposition, case study at Ziway-Shala basin, central Main Ethiopian rift*. Heliyon, 6, e03292, doi: 10.1016/j.heliyon.2020.e03292.

Landing E., Geyer G. and Heldmaier W.; 2006: *Distinguishing eustatic and epeirogenic controls on Lower-Middle Cambrian boundary successions in west Gondwana (Morocco and Iberia)*. Sedimentology, 53, 899-918, doi: 10.1111/j.1365-3091.2006.00780.x.

Leblanc M.; 1973: *La tectonique du Précambrien II dans la région de Bou-Azzer (Anti-Atlas central).* Notes Mem. Serv. G*éol. Maroc*, 33, 59-91.

Leblanc M.; 1976: *A Proterozoic oceanic crust at Bou Azzer.* Nature, 206, 34-35.

Leblanc M.; 1977: *Synchronisme des faciès volcaniques («Précambrien III») et sédimentaires (Adoudounien) dans l'Infracambrien d'Alous (Anti-Atlas, Maroc)*. C. R. Acad. Sci., 284, 878-882.

Leblanc M. and Billaud P.; 1978: *A volcano-sedimentary copper deposit on a continental margin of Upper Proterozoic age: Bleida (Anti-Atlas, Morocco)*. Econ. Geol., 73, 1101-1111.

Leblanc M. and Lancelot J.R.; 1980: *Interprétation géodynamique du domaine pan-africain (Précambrien terminal) de l'Anti-Atlas (Maroc) à partir de données géologiques et géochronologiques*. Can. J. Earth Sci., 17, 142-155, doi: 10.1139/e80-012.

Menke W.; 1989: *Geophysical data analysis: discrete inverse theory*. International Geophysics, Book Series, Menke W. (ed), Elsevier, Amstersam, The Netherlands, Vol. 45, 297 pp.

Michard A.; 1976: *Eléments de géologie marocaine*. Notes Mem. Serv. Géol. Maroc, 252, 408 pp.

Mokhtari A.; 1993: *Nouvelles données et interprétations du massif basique de Tagmout (dj. Saghro, Anti-Atlas, Maroc): relations avec les granitoïdes associés*. PH.D. Thesis in Earth Sciences, III cycle, Université Henri Poincaré, Nancy, France, 230 pp.

Mouge P. and Galdeano A.; 1991: *Magnetic mapping of the western Alps: compilation and geological implications*. Tectonophys., 190, 155-172, doi: 10.1016/0040-1951(91)90428-U.

Nabighan M.N.; 1972: *The analystic signal of two dimensional magnetic bodies with polygonal cross-section; its properties and use or automatic interpretation.* Geophys., 37, 507-517.

Nait Bba A., Boujamaoui M., Amiri A., Hejja Y., Rezouki I., Baidder L., Inoubli M.H., Manar A. and Jabbour H.; 2019: *Structural modeling of the hidden parts of a Paleozoic belt: insights from gravity and aeromagnetic data (Tadla basin and Phosphates plateau, Morocco)*. J. Afr. Earth Sci., 151, 506-522.

Phillips J.D.; 2000: *Locating magnetic contacts: a comparison of the horizontal gradient, analytic signal, and local wavenumber methods*. In: Expanded Abstracts SEG International Exposition and 70th Annual International Meeting, Calgary, AB, Canada, pp. 402-405, doi: 10.1190/1.1816078.

Piqué A.; 2003: *Evidence for an important extensional event during the Latest Proterozoic and Earliest Paleozoic in Morocco*. Comptes Rendus Geosci., 335, 865-868, doi: 10.1016/j.crte.2003.08.005.

Piqué A., Bouabdelli M., Soulaimani A., Youbi N. and Iliani M.; 1999: L*es conglomerates du P III (NéoProtérozoïque supérieur) de l'Anti-Atlas (sud du Maroc): molasses panafricaines, ou marqueurs d'un rifting fini-Protérozoïque?* C. R. Acad. Sci., 328, 409-414.

Piqué A., Soulaimani A., Hoepffner C., Bouabdelli M., Laville E., Amrhar M. and Chalouan A.; 2006: *Geologie du Maroc*. Editions Géode, Marrakech, Morocco, 280 pp.

Salako KA.; 2014: *Depth to basement determination using Source Parameter Imaging (SPI) of aeromagnetic data: an application to upper Benue trough and Borno basin, northeast, Nigeria*. Acad. Res. Int., 5, 74-80.

Saquaque A., Benharref M., Abia H., Mrini Z., Reuber I. and Karson J.A.; 1992: *Evidence for a Panafrican volcanic arc and wrench fault tectonics in the Jbel Saghro, Anti-Atlas, Morocco*. Geol. Rundsch., 81, 1-13, doi: 10.1007/BF01764536.

Schön J.H.; 2015: *Density*. In: Physical Properties of Rocks, Fundamentals and Principles of Petrophysics, 2nd ed., Elsevier, Amstersam, The Netherlands, pp. 109-118, doi: 10.1016/b978-0-08-100404-3.00004-4

Sharpton V.L., Grieve R.A.F., Thomas M.D. and Halpenny J.F.; 1987: *Horizontal gravity gradient: an aid to the definition of crustal structure in north America*. Geophys. Res. Lett., 14, 808-811, doi: 10.1029/gl014i008p00808.

Smith R.S., Thurston B., Dai T. and MacLeod I.N.; 1998: *iSPI™ - the improved source parameter imaging method*. Geophys. Prospect., 46, 141-151, doi: 10.1046/j.1365-2478.1998.00084.x.

Soulaimani A., Bouabdelli M. and Piqué A.; 2003: *L'extension continentale au Néo-Protérozoïque supérieur-Cambrien inférieur dans l'Anti-Atlas (Maroc)*. Bull. Soc. Géol. Fr., 174, 83-92.

Soulaimani A., Michard A., Ouanaimi H., Baidder L., Raddi Y., Saddiqi O. and Rjimati E.C.; 2014: *Late Ediacaran - Cambrian structures and their reactivation during the Variscan and Alpine cycles in the Anti-Atlas (Morocco)*. J. Afr. Earth Sci., 98, 94-112. doi: 10.1016/j.jafrearsci.2014.04.025.

Stampfli G.M. and Borel G.D.; 2002: *A plate tectonic model for the Paleozoic and Mesozoic constrained by dynamic plate boundaries and restored synthetic oceanic isochrones*. Earth Planet. Sci. Lett., 196, 17-33.

Thurston J.B. and Smith R.S.; 1997: *Automatic conversion of magnetic data to depth, dip, and susceptibility contrast using the SPI (TM) method*. Geophys., 62, 807-813.

Vanié L.T.A., Khattach D. and Houari M.R.; 2005: *Apport des filtrages des anomalies gravimétriques à l'étude des structures profondes du Maroc oriental*. Bull. Inst. Sci., Rabat, section Science de la Terre, 27, 29-40.

Zeng H., Xu D. and Tan H.; 2007: *A model study for estimating optimum upward-continuation height for gravity separation with application to a Bouguer gravity anomaly over a mineral deposit, Jilin province, northeast China*. Geophys., 72, I45-I50, doi: 10.1190/1.2719497.

Corresponding author: Assia Idrissi
Department of Earth Sciences, Faculty of Sciences, Mohamed V University
4 Ibn Batouta street, B.P. 1014 RP, Rabat, Morocco
Phone: +212 615630385; e-mail: idrissi.assia@gmail.com